Supplementary Discussion

Suga et al.[1] recently demonstrated that anterior pituitary gland tissue could be induced in a modified SFEBq culture. Both anterior pituitary and inner ear are derivatives of the non-neural ectoderm and, later, the pre-placodal region (PPR) of the head ectoderm. The anterior pituitary gland, however, is derived from the anterior most segment of the PPR whereas the inner ear is derived from the posterior PPR. In order to selectively induce anterior ectoderm, Suga et al. made two critical modifications to the original SFEBq culture. First, they used a medium devoid of any factors that influence tissue patterning, which has been shown previously to allow the induction of anterior neuroectoderm epithelia similar to the developing hypothalamus. Secondly, they seeded more ESCs (10,000 or greater) in each well to create a larger cell aggregate. In the large cell aggregate configuration a self-organizing non-neural epithelium was induced on the surface of the aggregate, while a neuroectoderm layer developed inside the aggregate. The authors speculated that the increased number of cells likely sets up a microenvironment permissive of the finely tuned BMP signaling that leads to non-neural and neuroectoderm induction *in vivo*. Importantly, they showed that treating smaller cell aggregates (3,000 cells) with BMP induced non-neural markers, however, the authors abandoned this approach for the large aggregate configuration. In the present study, we sought to gain better experimental control of non-neural ectoderm induction by applying BMP and a TGFβ inhibitor to the small cell aggregates. Additionally, we used a medium containing knockout serum replacement, which is permissive of posterior neuroectoderm induction in the presence of fibroblast growth factor[2,3]. We conjectured that this posteriorizing effect would translate to non-neural ectoderm tissue. Together, the non-neural induction strategies used by Suga et al. and in the present study provide mechanistic insight into how to derive placodes along the anterior-posterior axis.

Supplementary Figures and Legends

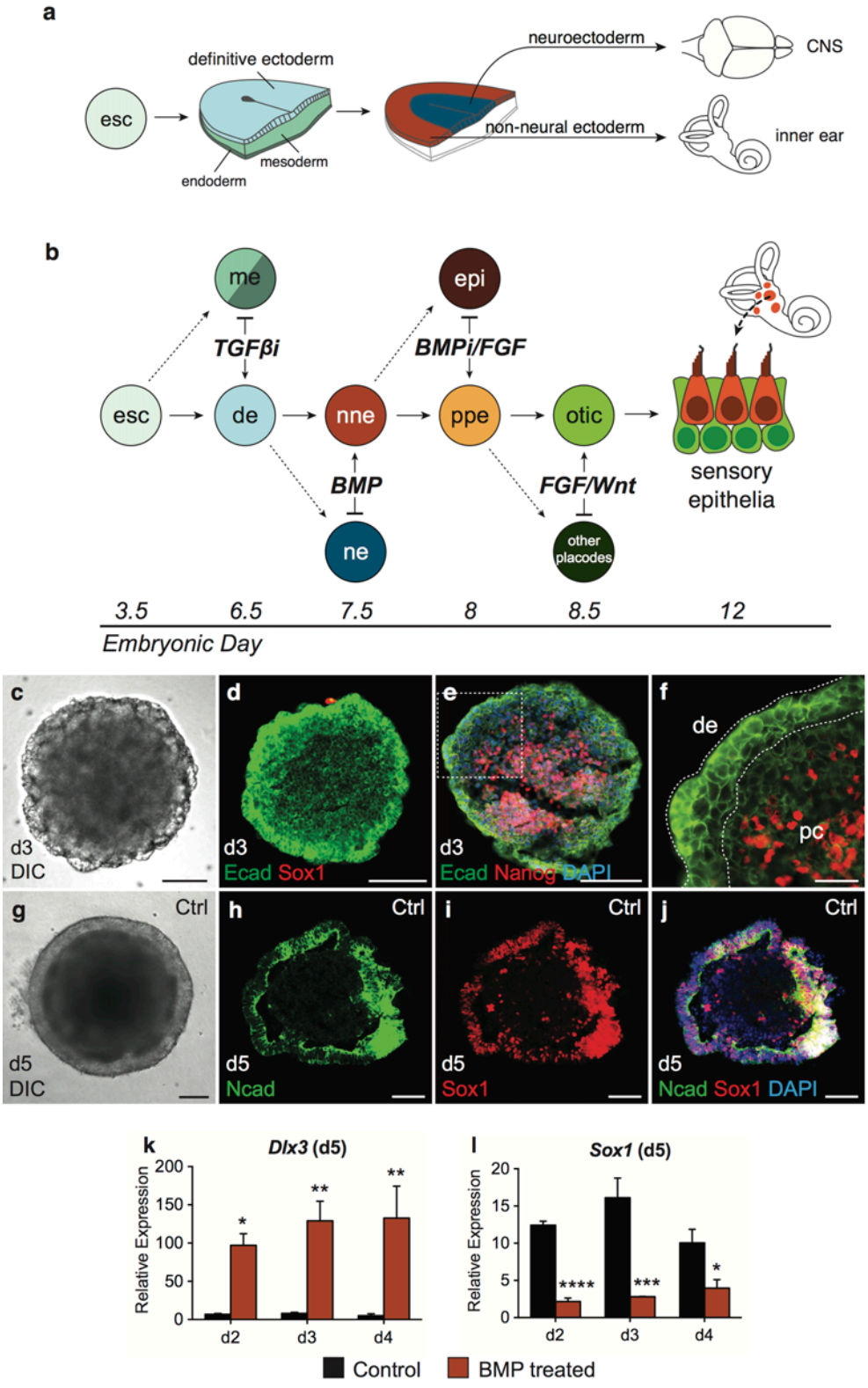

Supplementary Figure 1. Inner ear development from the definitive ectoderm.
a, The cell fate decision between non-neural ectoderm and neuroectoderm is the critical point of departure between central nervous system and inner ear development. **b**, The key cell fate decisions and inductive cues during inner ear development *in vivo* and in our *in vitro* culture system. Here "otic" refers specifically to prosensory cells found in the otic placode/vesicle that give rise to sensory epithelia containing hair cells and supporting cells. "Other placodes" refers to the adenohypophyseal, olfactory, lens, trigeminal, and epibranchial placodes, which are derived from more anteriorly located regions of the pre-placodal ectoderm. **c-f,** On day 3 of SFEBq differentiation, a Nanog/Sox1^{-} and Ecad^{+} epithelium forms on the outer surface of each aggregate. SFEBq has been shown to generate a nearly pure population of neuroectodermal cells (see Eiraku et al. 2008, 2011 and Kamiya et al. 2011); therefore, this epithelium may be roughly equivalent to embryonic definitive ectoderm because it is in-between a state of pluripotency (Nanog^{+}) and neuroectoderm (Sox1/Ncad^{+})[4-6]. To our knowledge, however, no *unique* markers of the definitive ectoderm are known. esc, embryonic stem cells; me, mesendoderm; de, definitive ectoderm; nne, non-neural ectoderm; ne, neuroectoderm; ppe, preplacodal ectoderm; epi, epidermis; otic, otic placode; pc, pluripotent cell.

g-j, By day 5 of differentiation, vehicle control (Ctrl) aggregates develop a Ncad/Sox1^{+} epithelium similar to the neuroectoderm *in vivo* and previous reports using SFEBq culture (see Eiraku et al. 2008, 2011 and Kamiya et al. 2011)[4-6]. **k-m,** qPCR analysis of day 5 samples after the addition of 10 ng/mL BMP or a vehicle control to the medium on day 2, 3 and 4. The non-neural ectoderm and mesendodermal markers *Dlx3* was upregulated in response to BMP4 treatment, whereas the neuroectodermal marker *Sox1* was downregulated (n=3; mean ± s.e.m.). A two-way ANOVA with Bonferroni's post hoc test for multiple comparisons was used to determine significance (*P<0.05, **P<0.01, ***P<0.001, ****P<0.0001). No significant differences were observed between control groups. Scale bars, 100 μm (**c-e**), 25 μm (**f**).

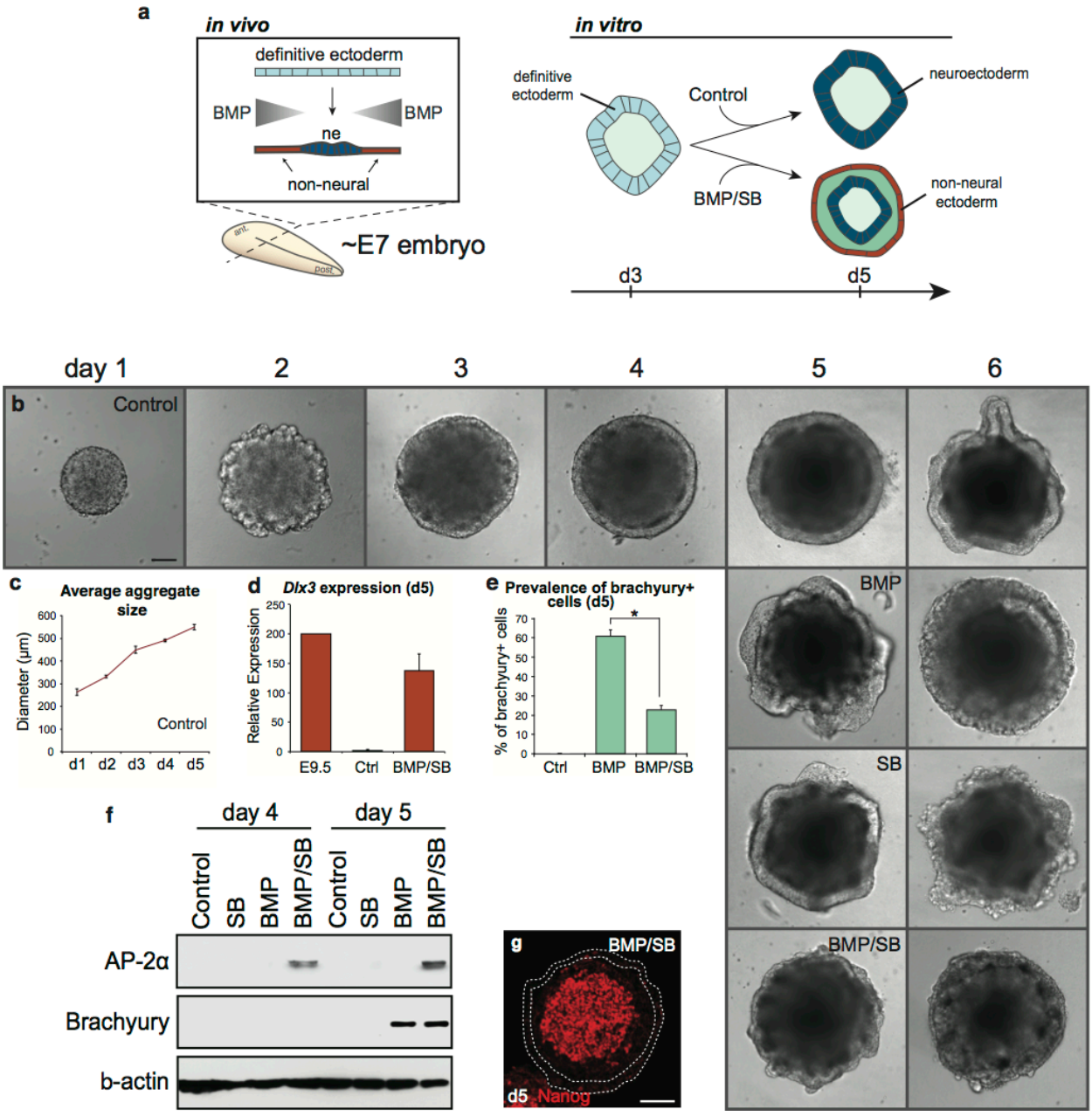

Supplementary Figure 2. Formation of non-neural ectoderm by BMP/SB treatment. **a,** The induction of non-neural ectoderm *in vivo* by a BMP gradient can be recapitulated *in vitro* by treating day 3 SFEBq aggregates with BMP and SB. **b,** Overt morphological changes occur in BMP, SB and BMP/SB treated aggregates beginning on day 5. Note that the epithelium is disrupted in BMP and SB treated aggregates, while a thin epithelium can be observed along the outer edge of day 5 and 6 BMP/SB treated aggregates. Data are representative of 4-12 separate experiments. **c**, The average size of ESC aggregates increases during the first 5 days of differentiation (n=10; mean ± s.e.m.). **d**, *Dlx3* expression was induced following BMP/SB treatment (n=6, 2 separate experiments; mean ± s.d.). **e,** The percentage of brachyury^{+} cells decreased significantly following BMP/SB treatment versus BMP treatment (n=9, 3 separate experiments; *P<0.05; mean ± s.e.m.). **f,** Western blot analysis reveals that AP2 protein is only

detectable in BMP/SB treated aggregates beginning on day 4 (i.e. 24 hours after treatment). Consistent with qPCR and immunostaining, brachyury is detectable on day 5 in both BMP and BMP/SB treated aggregates. **g**, Nanog expression is restricted to the core of each BMP/SB aggregate on day 5. Scale bars, 100 μm (**b, g**).

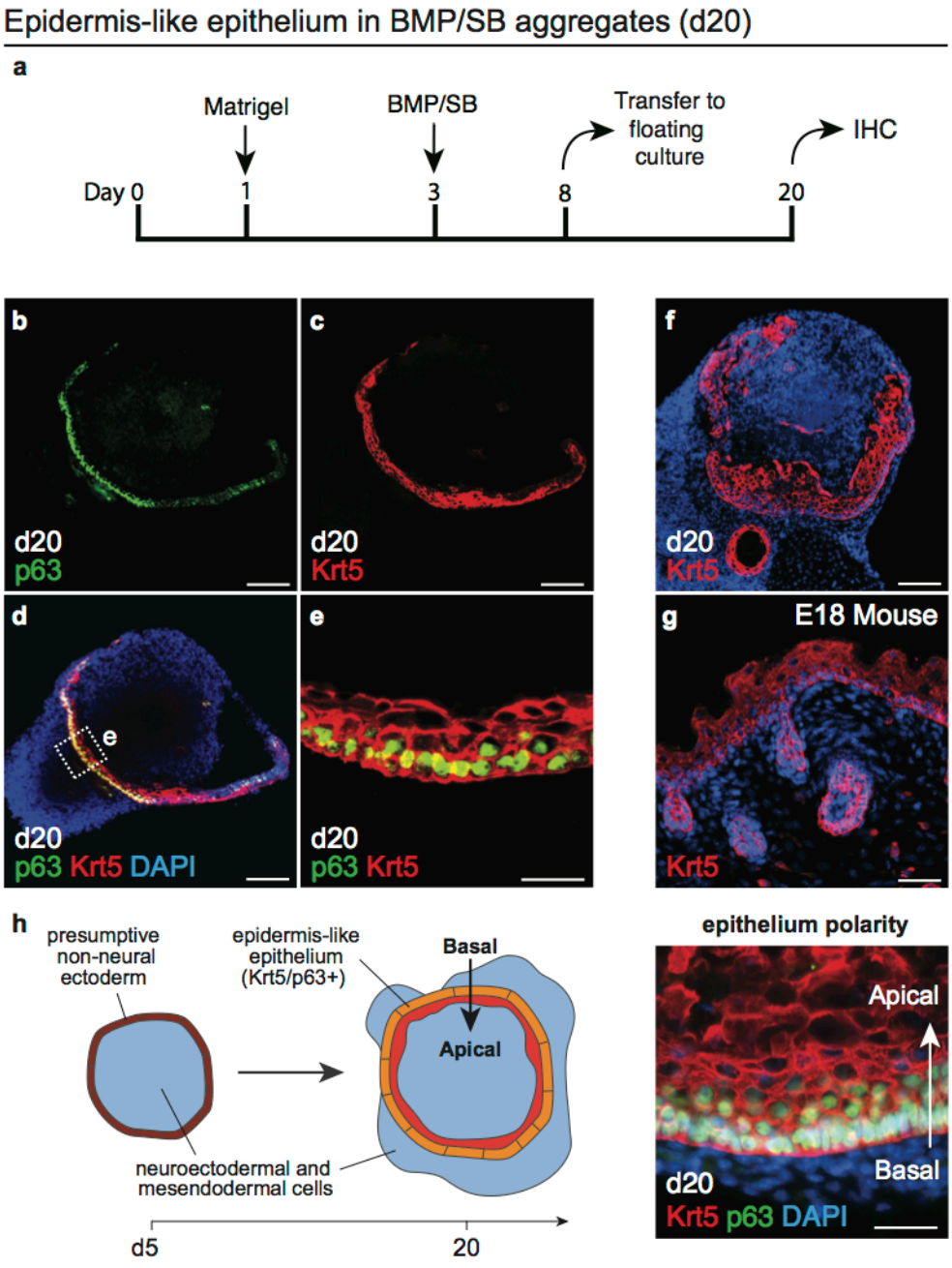

Supplementary Figure 3. Long-term culture of BMP/SB samples generates epidermis. **a**, Following 8 days of differentiation in 96-well plates, BMP/SB aggregates were washed with N2 Medium and transferred to floating culture for self-guided development. **b-e**, A Krt5/p63^{+} epithelium develops in BMP/SB aggregates cultured for 20 days. These results were confirmed in 3 separate experiments. **f, g,** The staining pattern and morphology of the Krt5^{+} epithelium is consistent with epidermis on the surface of E18 mouse embryos **h,** The basal to apical polarity of the epidermis is oriented toward the interior of the aggregate. These results are consistent with *in vivo* induction of epidermis from the non-neural ectoderm. Interestingly, BMP/SB treatment on day 3 appears to be necessary and sufficient to initiate self-organized induction of epidermis. No

Krt5/p63^{+} epithelium was observed in vehicle treated aggregates (data not shown). Scale bars, 100 μm (**b-c, f, g**), 25 μm (**e, h**).

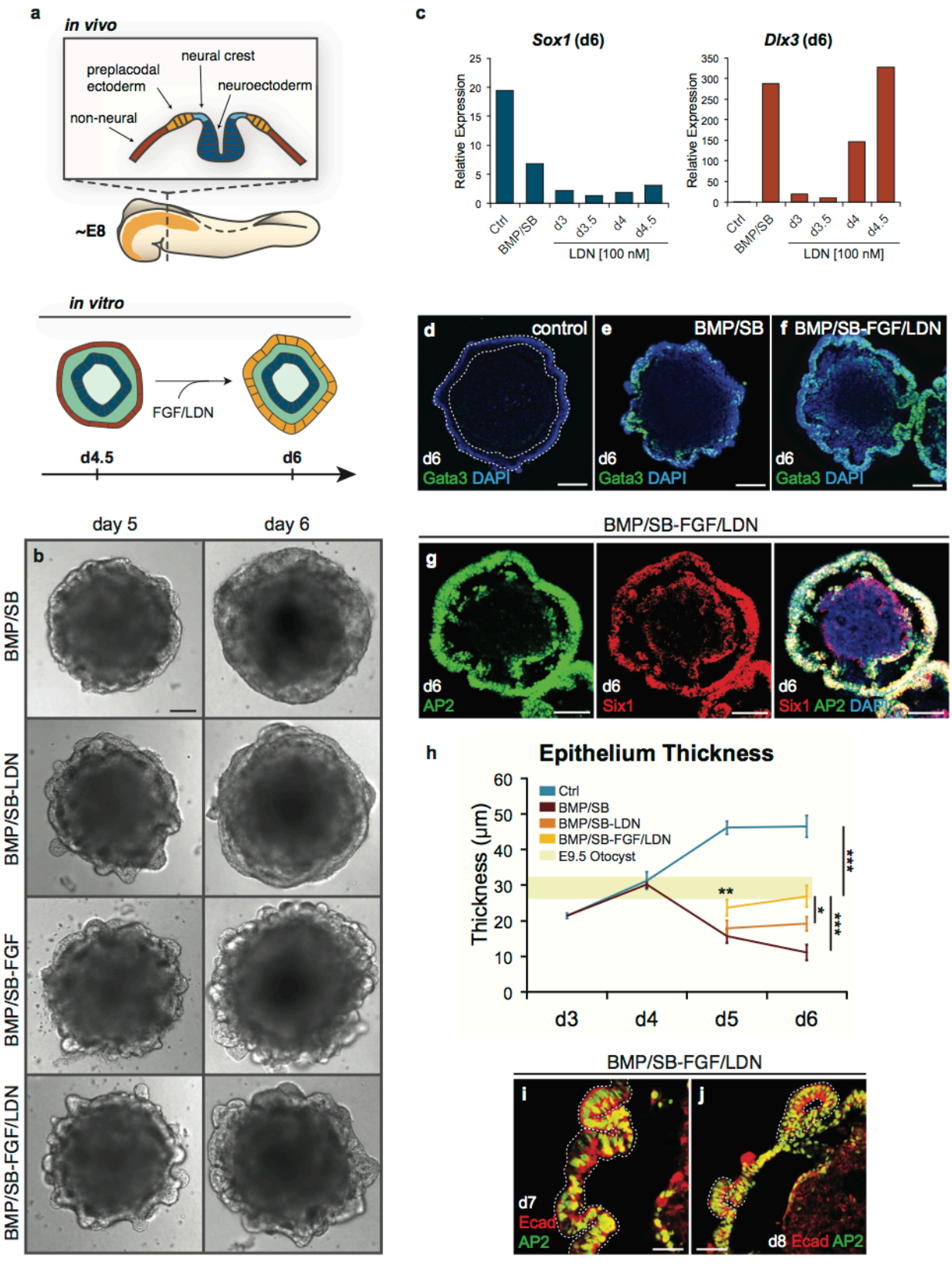
a
in vivo
neural crest
preplacodal ectoderm
neuroectoderm
non-neural
~E8
in vitro
FGF/LDN
d4.5
d6
c
Sox1 (d6)
Dlx3 (d6)
Relative Expression
Ctrl
BMP/SB
d3
d3.5
d4
d4.5
LDN [100 nM]
d control
e BMP/SB
f BMP/SB-FGF/LDN
d6
Gata3 DAPI
BMP/SB-FGF/LDN
g
AP2
Six1
Six1 AP2 DAPI
day 5
day 6
b
BMP/SB
BMP/SB-LDN
BMP/SB-FGF
BMP/SB-FGF/LDN
h
Epithelium Thickness
Thickness (µm)
Ctrl
BMP/SB
BMP/SB-LDN
BMP/SB-FGF/LDN
E9.5 Otocyst
d3
d4
d5
d6
i
j
d7
Ecad
AP2
d8 Ecad AP2

Supplementary Figure 4. Epithelium characteristics following BMP/SB–FGF, -LDN and -FGF/LDN treatment.

a, The induction of pre-placodal ectoderm *in vivo* by BMP inhibitors and FGFs can be recapitulated *in vitro* by treating day 4-5 BMP/SB aggregates with LDN-193189 and FGF2. **b**, Morphological changes occur following BMP/SB-LDN, -FGF and -FGF/LDN treatment on days 5 and 6. **c**, LDN treatment does not induce *Sox1* expression, but suppresses *Dlx3* expression if treatment occurs on or before day 4 (data are representative of 2 separate experiments). **d-g,** Gata3 (**d-f**) and Six1 **(g)** were detected in the outer epithelium of BMP/SB and BMP/SB-FGF/LDN treated aggregates. **h,** The apparent thicknesses of Control, BMP/SB, BMP/SB-LDN and BMP/SB-FGF/LDN epithelia on days 3-6. For comparison, the apparent thickness of the E9.5 otic vesicle is superimposed. Data represent 15-20 aggregates from 3-4 separate experiments and 6 otocysts from 3 embryos (mean ± s.e.m.). A one-way ANOVA was used to determine significant differences between groups (**P*<0.05, ***P*<0.01, ****P*<0.001). On day 5, BMP/SB-FGF/LDN was significantly different from all other groups. **i, j**, Epithelium ruffling and vesicle formation on day 7 and 8 following BMP/SB-FGF/LDN treatment. Scale bars, 100 μm (**d-g**), 50 μm (**g**), 25 μm (**d, f**)

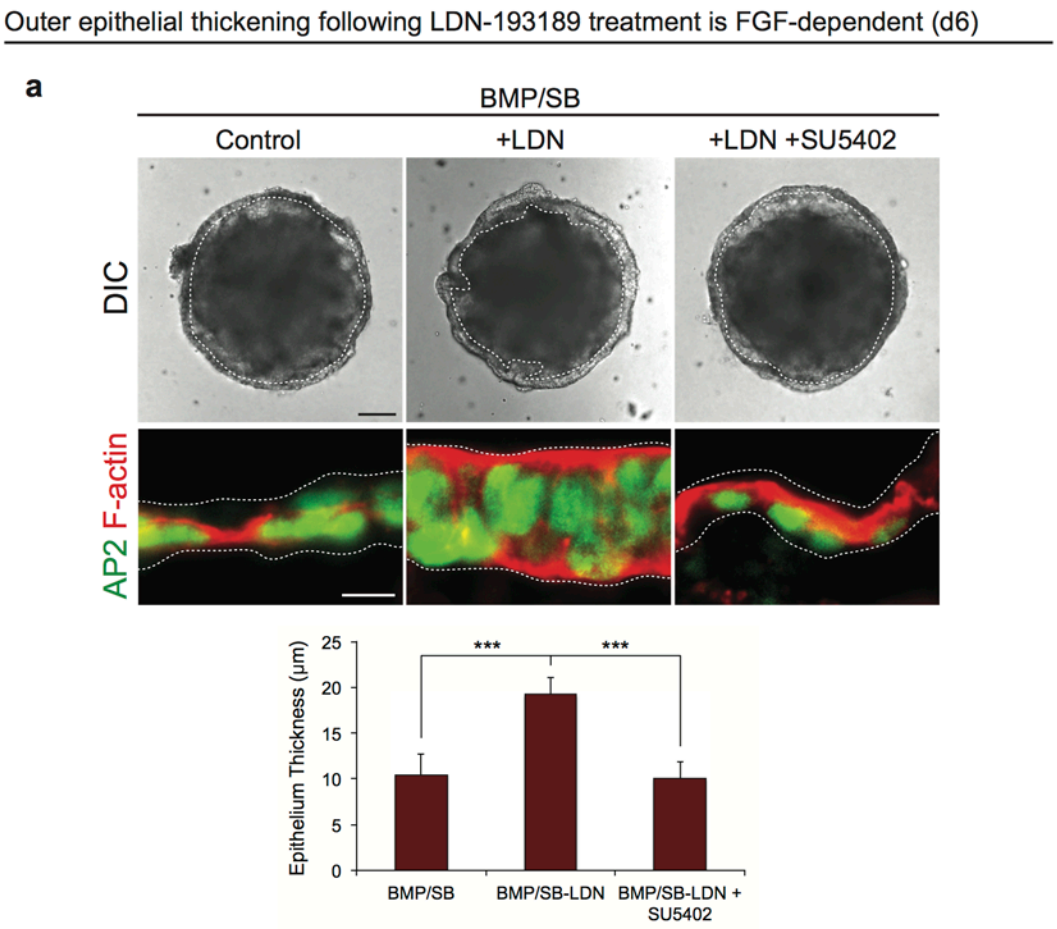

Supplementary Figure 5. Epithelial thickening is FGF-dependent and Pax8 expression is dependent on FGF dosage.

a, Inhibition of FGF using SU5402, abolishes epithelial thickening following BMP/SB-LDN treatment (n=9 aggregates, 3 separate experiments, ***P<0.001). AP2 expression, however, is

still found in the outer epithelium following SU5402 treatment. **b**, qPCR analysis shows that *Pax8* expression is dependent on FGF dosage. FGF dosages >25 ng/mL showed an upward trend in *Pax8* expression, however, differences between 25, 50 and 100 ng/mL were not significant using a one-way ANOVA with Tukey's post hoc test for multiple comparisons. 25 ng/mL was chosen as the appropriate dosage for all subsequent experimentation (n=4, **P*<0.05, ***P*<0.01, ****P*<0.001; mean ± s.e.m.). Scale bars, 100 μm (**a**, top panels) and 10 μm (**a**, middle panels).

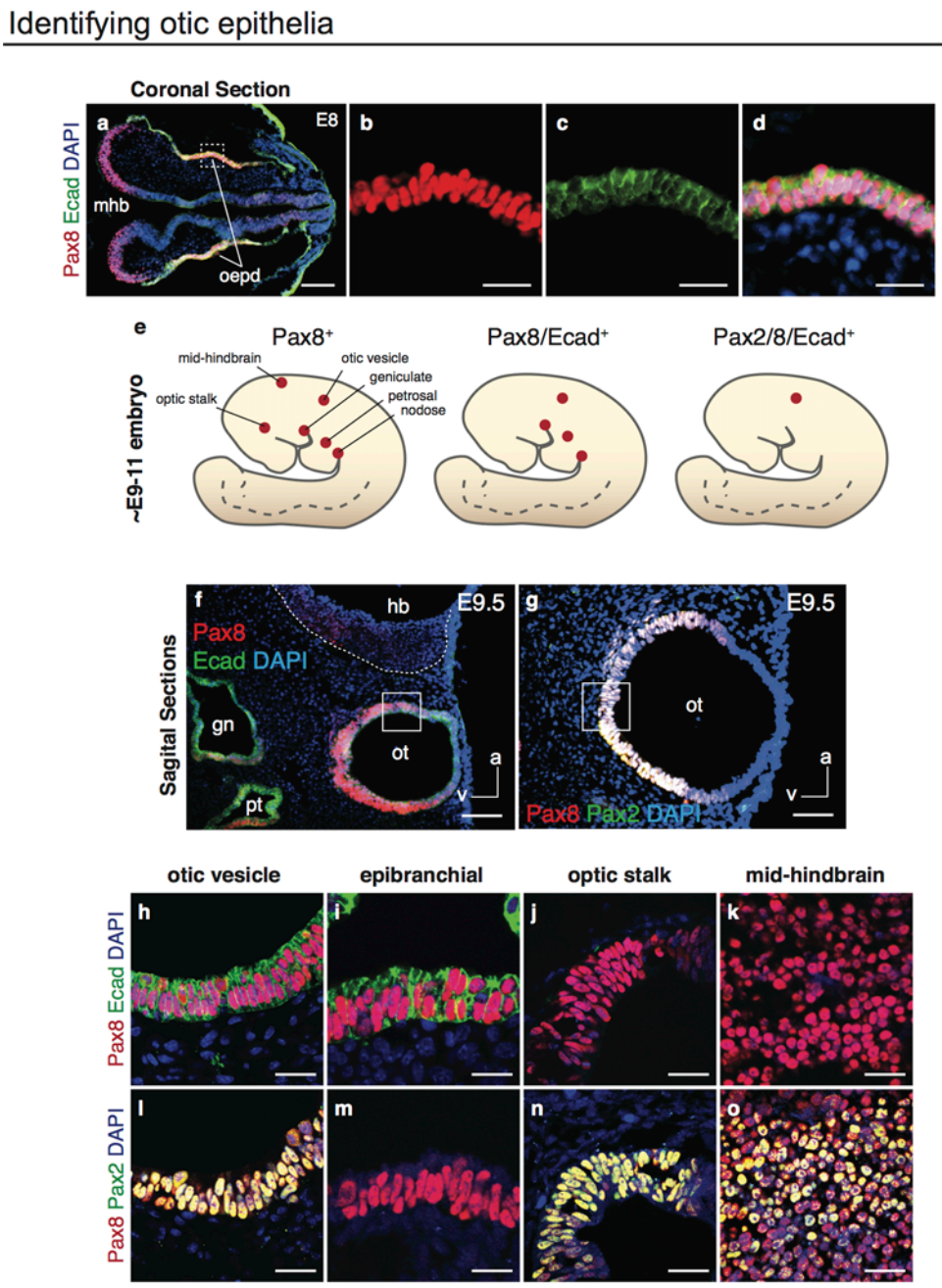

Supplementary Figure 6. Identifying otic progenitor cells.
a-d, At E8, Pax8/Ecad expression in the surface ectoderm marks the otic-epibranchial placode domain (oepd). Pax8 expression is also detected in the mid-hindbrain region of the neuroepithelium (mhb). **e-m**, The well-established otic markers Pax2/8 are not unique to the inner ear during development. On E9.5 Pax2/8 expression co-localizes in the optic stalk, mid-hindbrain and kidney as well as the otic vesicle. We found that the combination of Pax2/8 and Ecad provides a unique signature of otic placode/vesicle fate. At ~E9-11, **Pax8** is expressed in the otic vesicle, epibranchial placodes (i.e. geniculate, petrosal and nodose), optic stalk, and mid-hindbrain. **Pax8/Ecad** expression is restricted to the otic vesicle and epibranchial placodes.

Pax2/8/Ecad expression is restricted to the otic vesicle (**h**, **l**). a, anterior; v, ventral. Scale bars, 100 μm (**a, f, g**), 25 μm (**b-d, h-o**).

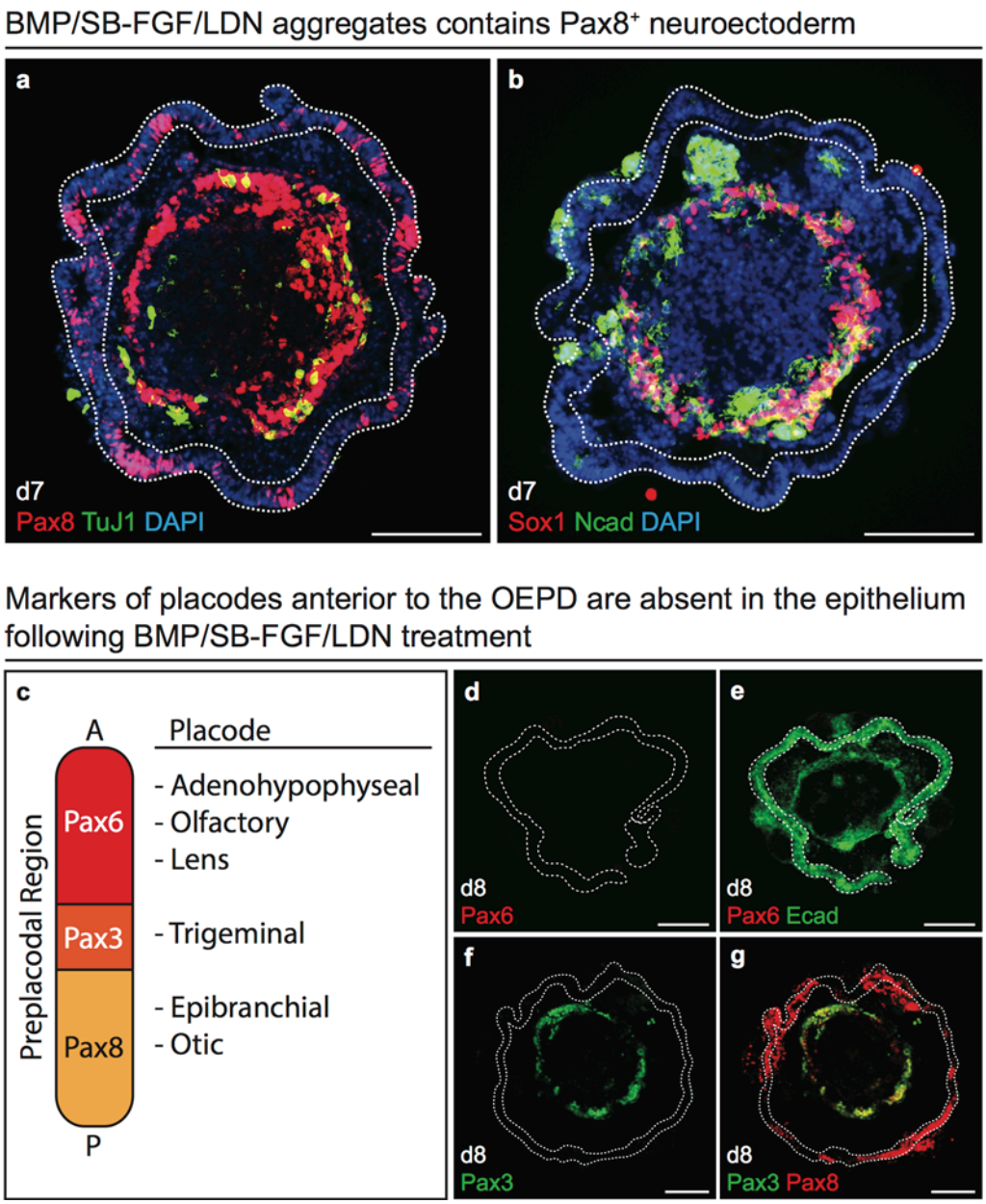

Supplementary Figure 7. The cellular composition and organization of BMP/SB-FGF/LDN treated aggregates.

a, **b**, An interior layer of Pax8 and Sox1/Ncad^{+} cells develops in BMP/SB-FGF/LDN aggregates. This expression pattern is consistent with developing mid-hindbrain tissue. Notably, ßIII-tubulin (TuJ1)$^{+}$ neurons developed within this region, confirming a neural identity. **c**, In the pre-placodal region of the embryo, Pax6 expression delineates the anterior placodes (i.e. the adenohypopheseal, olfactory and lens placodes), whereas Pax3 is expressed in the trigeminal placode. **d**, **e**, Pax6 is not expressed in day 8 BMP/SB-FGF/LDN treated aggregates. **f**, **g**, Pax3 is expressed in Pax8^{+} cells located in the interior layer, however, no Pax3 expression was observed in the outer-epithelium. Scale bars, 100 µm.

We speculate that FGF/LDN treatment guides cell fate specification at multiple layers of the aggregates. In the outer epithelium, FGF/LDN induces a pre-placode-like epithelium and,

specifically, an epithelium similar to that of the OEPD. Comparably, FGF/LDN appears to act on an inner layer of neuroectodermal cells to induce mid-hindbrain-like tissue. It is likely that the insulin content of Knockout Serum Replacement contributes to the caudalizing affect of FGF/LDN treatment. Previously, insulin and FGF2 were used to induce mid-hindbrain in SFEBq culture (Muguruma et al., 2010)[3]. Likewise, mechanosensitive hair cells were previously derived using, in part, insulin-like growth factor and FGF2 (Oshima et al., 2010)[7].

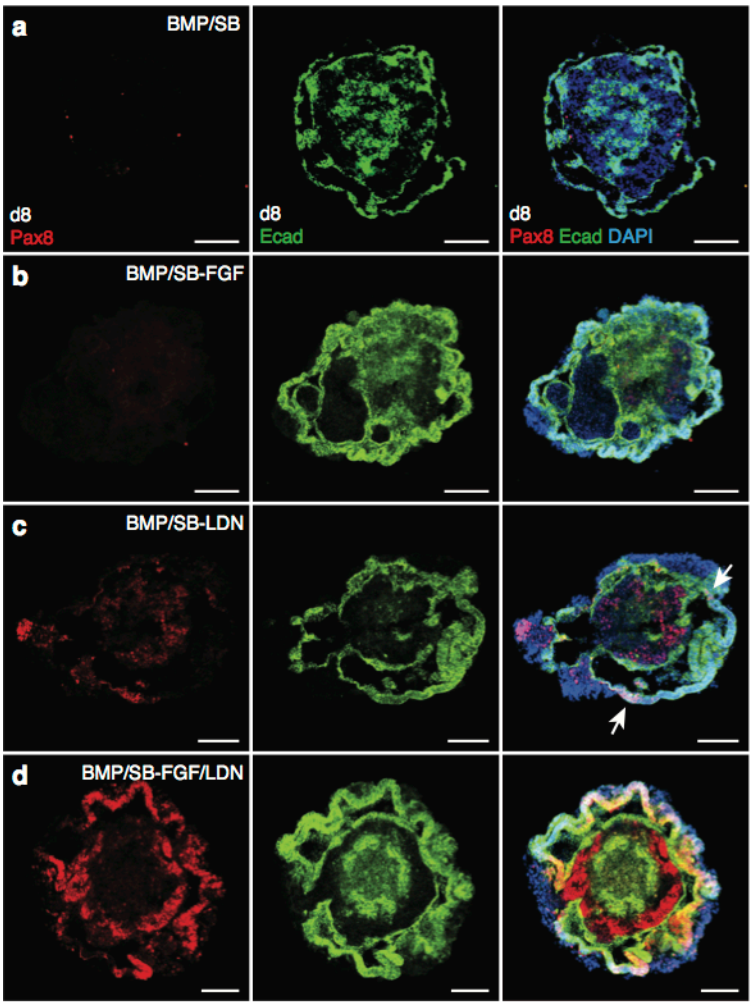
a
BMP/SB
d8
Pax8
d8
Ecad
d8
Pax8 Ecad DAPI
b
BMP/SB-FGF
c
BMP/SB-LDN
d
BMP/SB-FGF/LDN

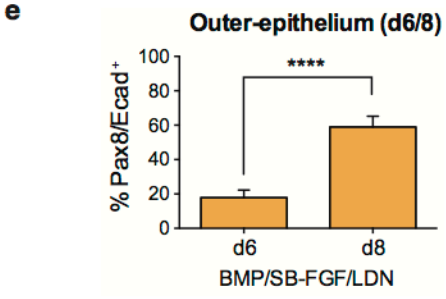
e
Outer-epithelium (d6/8)
% Pax8/Ecad+
100
80
60
40
20
0
****
d6
d8
BMP/SB-FGF/LDN

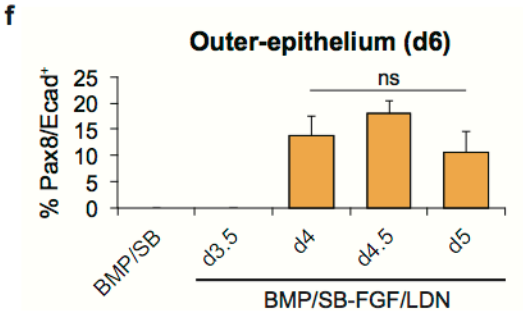
f
Outer-epithelium (d6)
% Pax8/Ecad+
25
20
15
10
5
0
ns
BMP/SB
d3.5
d4
d4.5
d5
BMP/SB-FGF/LDN

Supplementary Figure 8. Necessity and proper timing of FGF/LDN treatment for Pax8 induction.

a-d, Representative immunostaining for Pax8/Ecad on day 8 of differentiation. For BMP/SB-LDN treated aggregates arrows identify the patches of Pax8/Ecad^{+} cells. We conclude from these results that the combined treatment of FGF/LDN or, potentially, LDN combined with endogenous FGFs is necessary to induce Pax8/Ecad^{+} epithelium. **e**, Percentage of Ecad^{+} epithelium expressing Pax8 on day 6 and 8 (n=9 aggregates, 3 separate experiments, ****P<0.0001, mean ± s.e.m.). For these experiments FGF/LDN treatment was performed on day 4.5. ns, not significant. Scale bars, 100 μm.

f, FGF/LDN treatment only generated Pax8/Ecad epithelium following treatment on days 4-5. FGF/LDN treatment after d5 did not result in epithelial thickening (data not shown). The graph shows quantification of the average percentage of Pax8/Ecad^{+} epithelium on day 6 (n=12 aggregates, 4 separate experiments; mean ± s.d.). Representative images for BMP/SB and BMP/SB-FGF/LDN can be found in Figure 2d and e.

Cellular re-organization during days 8-12 (BMP/SB-FGF/LDN sections only)

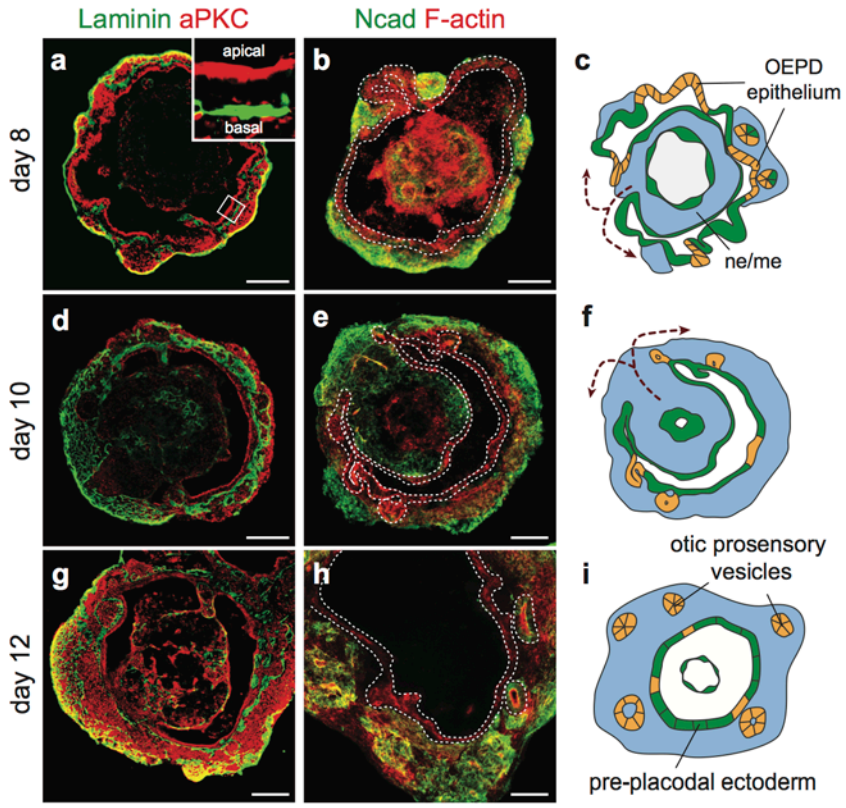

The degree of cellular re-organization differs between conditions

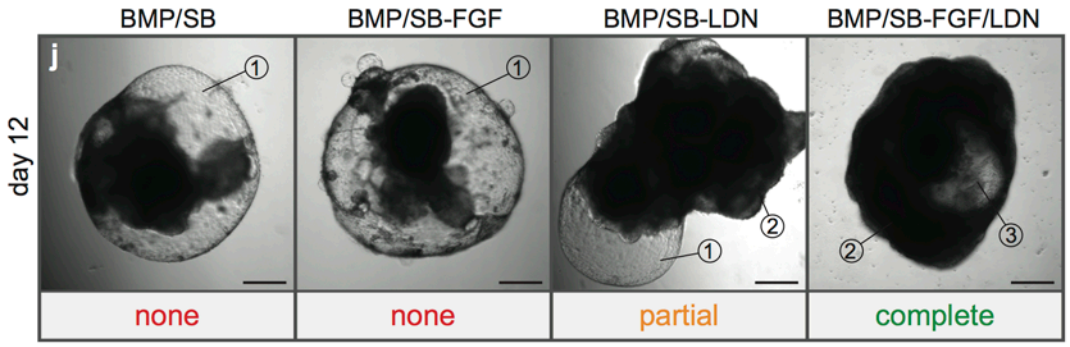

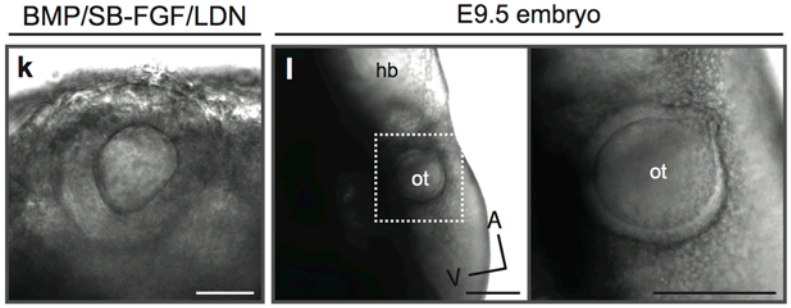

Supplementary Figure 9. Cellular re-organization and vesicle formation in BMP/SB-FGF/LDN aggregates.

a-i, To elucidate the process of cellular re-organization during days 8-12, aggregates were stained for basal (laminin) and apical (aPKC) polarity markers (**a, d, g**). Note that the basal surface of the epithelium remains oriented toward the outside of the aggregate as the inner cell mass relocates to the out surface of the aggregate. Ncad (a marker for both neuroectoderm and mesoderm *in vivo*) labeled most cells in the inner cell mass and helps visualize the topographical change (**b, e, h**) depicted in **c, f** and **l.** F-actin staining was used to identify the epithelium. Presumptive otic vesicles (dotted outline in **h**) express Ncad. **j**, Representative DIC images of aggregates on day 12 could be assessed for cellular re-organization based on morphology. Note the translucent epithelium found in all conditions except BMP/SB-FGF/LDN treated samples. (1) This translucent epithelium is indicative of incomplete or partial re-organization. (2) An opaque outer cell mass was indicative of partial or complete re-organization. (3) Fully re-organized aggregates display a hallow core that is clearly visible through the aggregate surface (images are representative of ~90-95% of aggregates for each condition; 4 experiments). **k**, From day 8-20, vesicles were visible under the surface of BMP/SB-FGF/LDN treated aggregates (day 12 shown). **l**, The embedded BMP/SB-FGF/LDN vesicles were comparable in appearance to the otic vesicle in E9.5 mouse embryos as viewed through the surface ectoderm. hb, hindbrain; ot, otic vesicle. Scale bars, 250 μm (**j, l**), 100 μm (**a-i**) 50 μm (**k**).

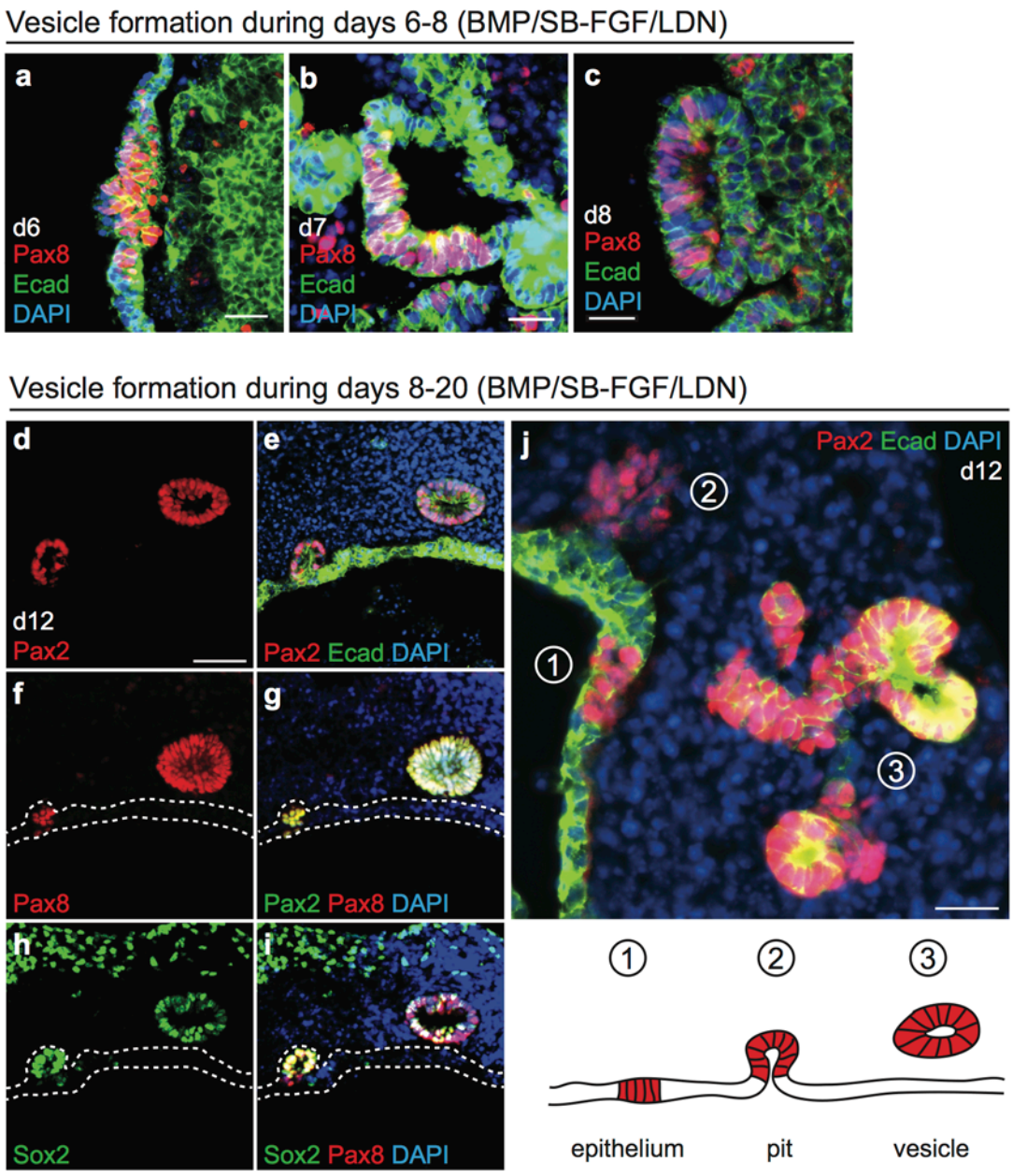

Supplementary Figure 10. Prosensory vesicle formation.
a-c, Pax8/Ecad^{+} vesicle formation from the outer epithelium during days 6-8. **d-i**, Serial sections show co-expression of Pax2/8, Ecad, and Sox2 in vesicles, indicating an inner ear prosensory fate. **j**, A fortuitous section of a day 12 aggregate illustrates the 3 steps of vesicle formation. Scale bars, 50 µm (**d-i**), 25 µm (**a-c**).

Note that vesicle formation appeared to be continuous beginning on day 7 until approximately day 14/16. We did not, however, determine the precise time that vesicle formation ceased.

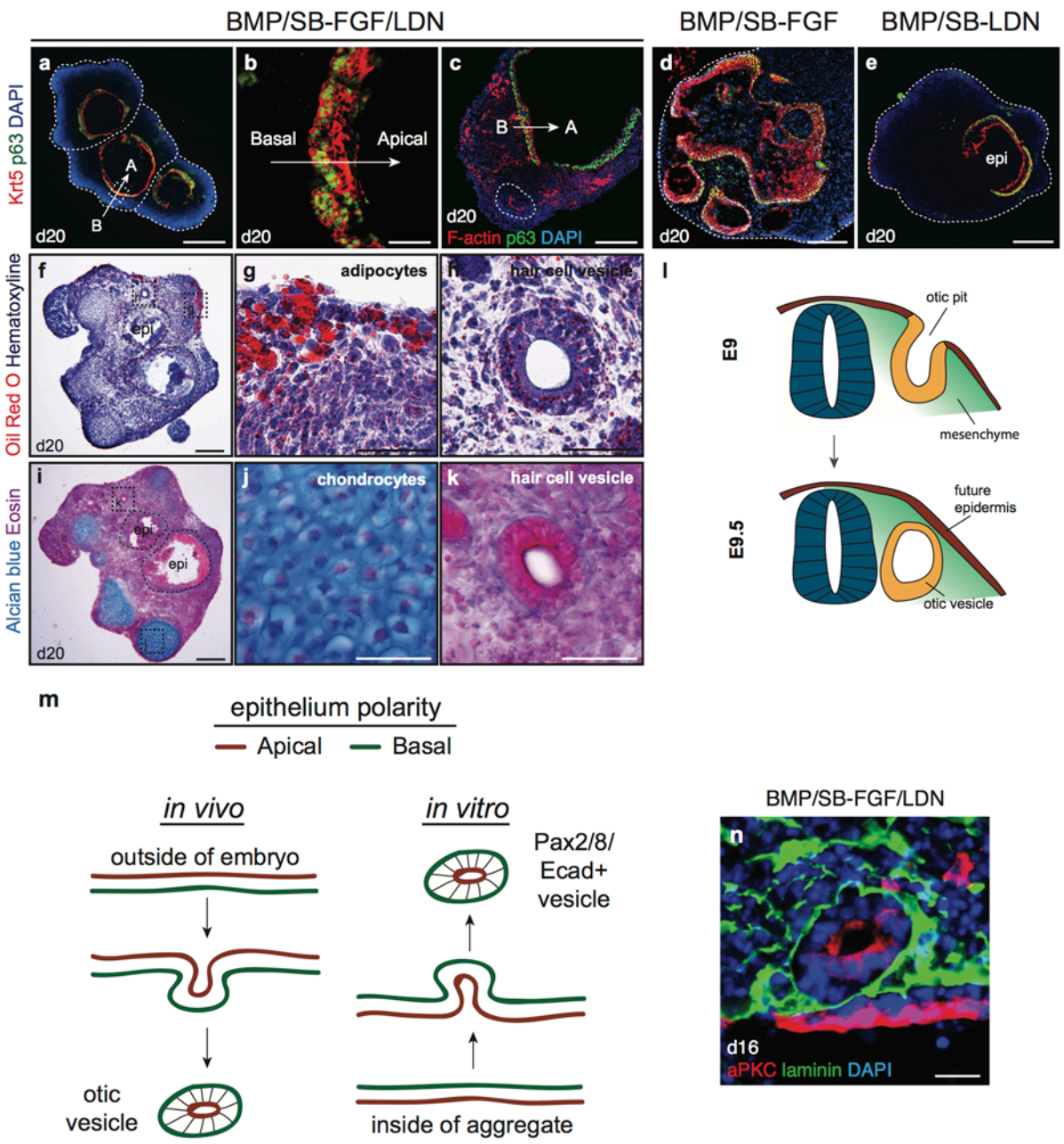

Supplementary Figure 11. Epidermis arises under all BMP/SB treated conditions and vesicles evaginate into mesenchyme-like tissue.
a-e, Krt5/p63^{+} epidermis-like epithelium forms in BMP/SB-FGF, -LDN and -FGF/LDN aggregates. In BMP/SB-LDN and BMP/SB-FGF/LDN aggregates the Krt5/p63^{+} epithelium lines the central cavity of the aggregate with the apical surface oriented toward the interior of the aggregate (**b**). F-actin staining with phalloidin reveals that vesicles (outlined) are located basal to the p63^{+} epithelium (**c**). **f-l**, Oil Red O and Alcian Blue staining shows that adipocytes and chondrocytes develop adjacent to hair cell-containing vesicles in the outer cell mass. This confirms that presence of mesenchymal development in this region of the aggregates. The

development of hair cell vesicles surrounded by mesodermal tissue in BMP/SB-FGF/LDN aggregates mimics the development of the inner ear in the head mesenchyme (**l**).

m, One apparent discrepancy between *in vitro* and *in vivo* otic vesicle formation is that the otic placode *invaginates* into the body to form the otic vesicle (**l**, ~E9-9.5) and, conversely, *in vitro* vesicles *evaginate* out into the medium or exterior cell layer. From the Krt5/p63 staining results, we can see that the basal-to-apical polarity of the inner epithelium is oriented outside-to-inside relative to the surface of BMP/SB-FGF/LDN aggregates (note that a similar orientation was observed in BMP/SB aggregates [Supplemental Fig. 3]). The schematic illustrates how vesicles that appear to *evaginate* toward the exterior of the aggregate *in vitro* are, in actuality, *invaginating* relative to the polarity of the epithelium. Staining for apical (aPKC) and basal (laminin) polarity markers (**n**) confirms this model. Scale bars, 250 μm (**a**), 100 μm (**c-f, i**), 50 μm (**g, h, j, k**) 25 μm (**b**,**n**).

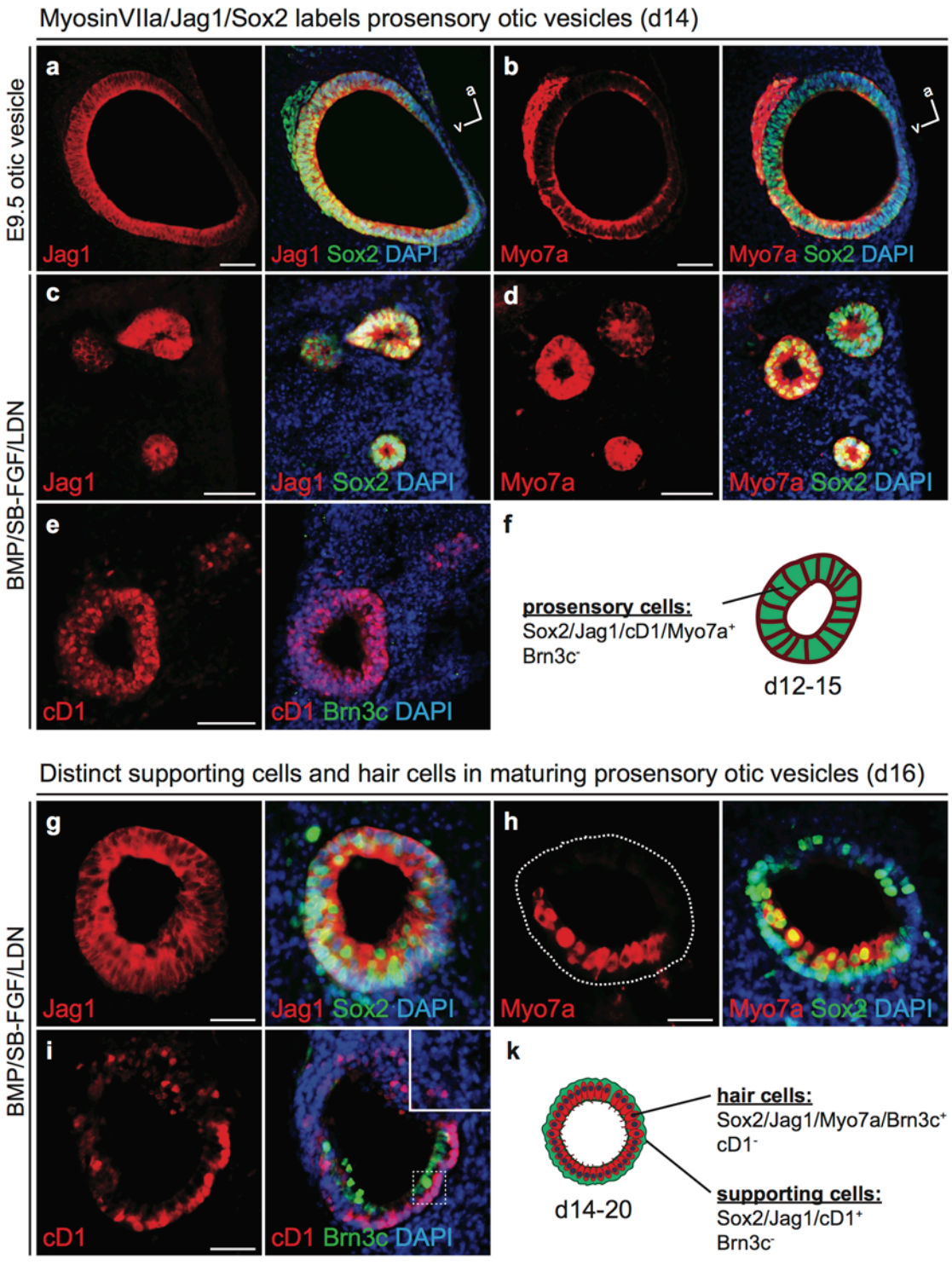

Supplementary Figure 12. Early hair cell induction (d14-16)
a-f, At day 14 of differentiation, prosensory vesicles express Sox2/Jag1/Myo7a, mimicking the expression pattern of the E9.5 otic vesicle. **e**, Prosensory cells also expressed cD1, but did not express the hair cell marker Brn3c. **g-k**, Maturing prosensory otic vesicles express Jag1/Sox2 in both supporting cells and hair cells, while Myo7a/Brn3c and cD1 expression in confined to hair

cells and supporting cells, respectively. **f, k**, Schematic showing the characteristics of prosensory otic vesicles observed between days d12-15 versus vesicles with further differentiated sensory epithelia containing hair cells and supporting cells observed between days 14-20. Scale bars, 50 μm (**a-e**), 25 μm (**g-i**).

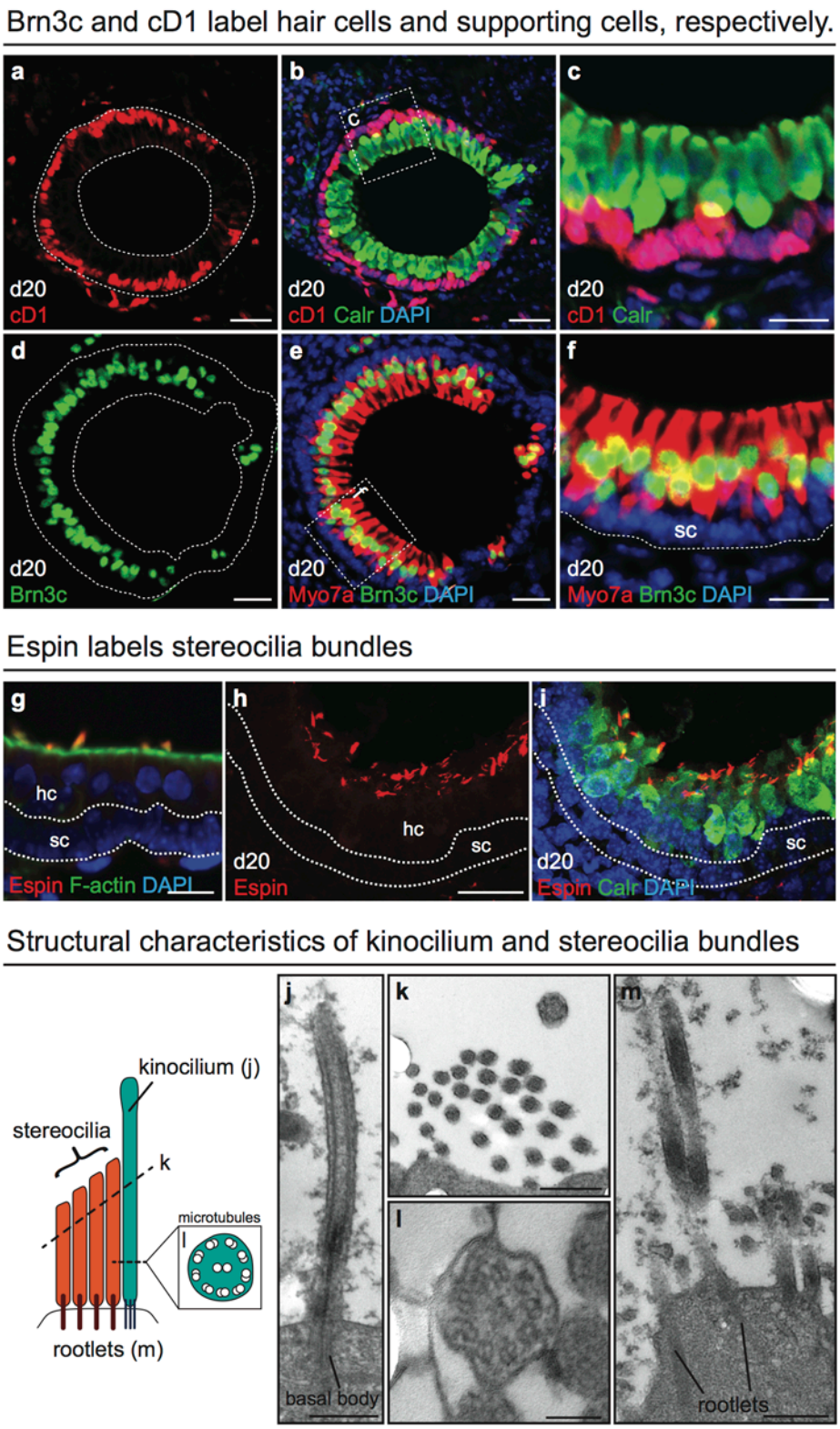

Supplementary Figure 13. Hair cell maturation (d16-20)
a-f, Brn3c and cD1 delineate hair cells from supporting cells in d20 epithelia. **g-i**, Stereocilia bundles express Espin, characteristic of stereocilia on authentic inner ear hair cells. **j-m**, Transmission electron microscopy reveals several ultrastructural hallmarks found in stem cell-

derived hair cells. Notably, a single kinocilium with basal body (**j, k**) was associated with each bundle of stereocilia (**k**). Cross-sections of kinocilia displayed the characteristic configuration of 9 microtuble doublets surrounding 2 central microtubules. Also, stereocilia have rootlets (**m**) that extended into the cell body. Scale bars, 25 μm (a**-i**), 500 nm (**j, k, m**), 100 nm (**l**).

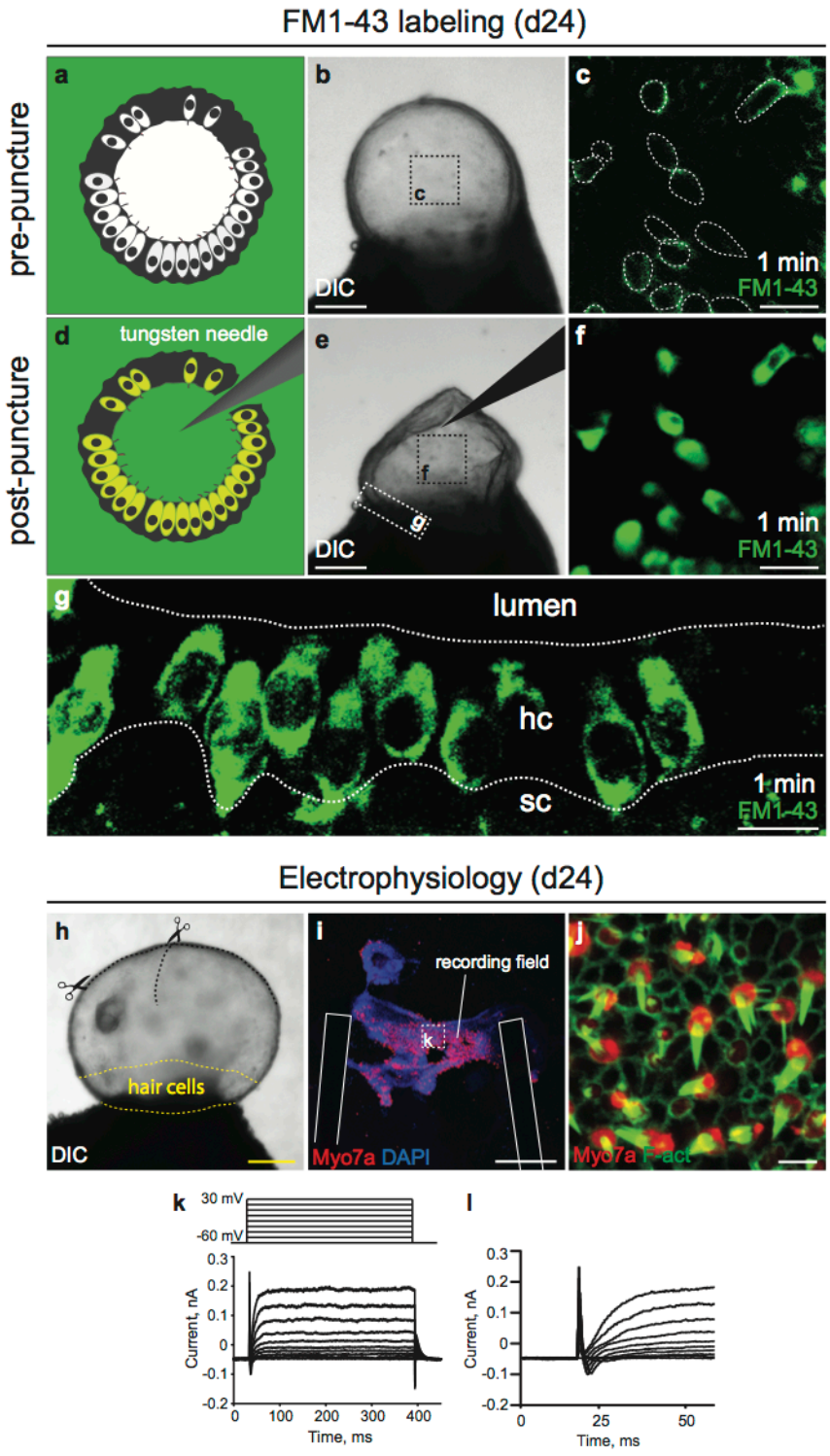

Supplementary Figure 14. Functional properties of stem cell-derived hair cells using a FM1-43 uptake assay and electrophysiological recordings.

a-c, Vesicles containing hair cells were identified by morphology as translucent cysts protruding from the side of cell aggregates. Hair cells in the epithelium could be identified through the vesicle wall following treatment with FM1-43FX for 1 minute. **d-g**, After puncturing the vesicle

with a 0.25 μm tungsten needle and another 1 minute incubation, previously outlined hair cells became fluorescent (**f**). Confocal imaging of the epithelial sheet revealed FM1-43FX labeled cells with the same morphology as hair cells. The underlying supporting cells did not take up the dye (**g**; sc). These results are consistent with previous investigations (see Meyers et al., 2003) and were confirmed using 10 vesicles from 3 different experiments[8].

h, For electrophysiological recording, vesicles were microdissected to flatten the sensory epithelium (typically found in the portion of the vesicle abutting the aggregate). **i**, The sensory epithelium was secured to a coverslip by two needles during recording. **j,** Post-recording, samples were fixed and stained for Myo7a and F-actin (phalloidin) to confirm the identity of hair cells. **k**, Representative traces of complex current which include the inward and outward components. The voltage protocol is shown at the top. **l,** Expanded view of transient inward current (likely calcium). Outward current was truncated for clarity. Scale bars, 250 μm (**b, e, h, i**), 25 μm (**c, f, g**), 5 μm (**j**).

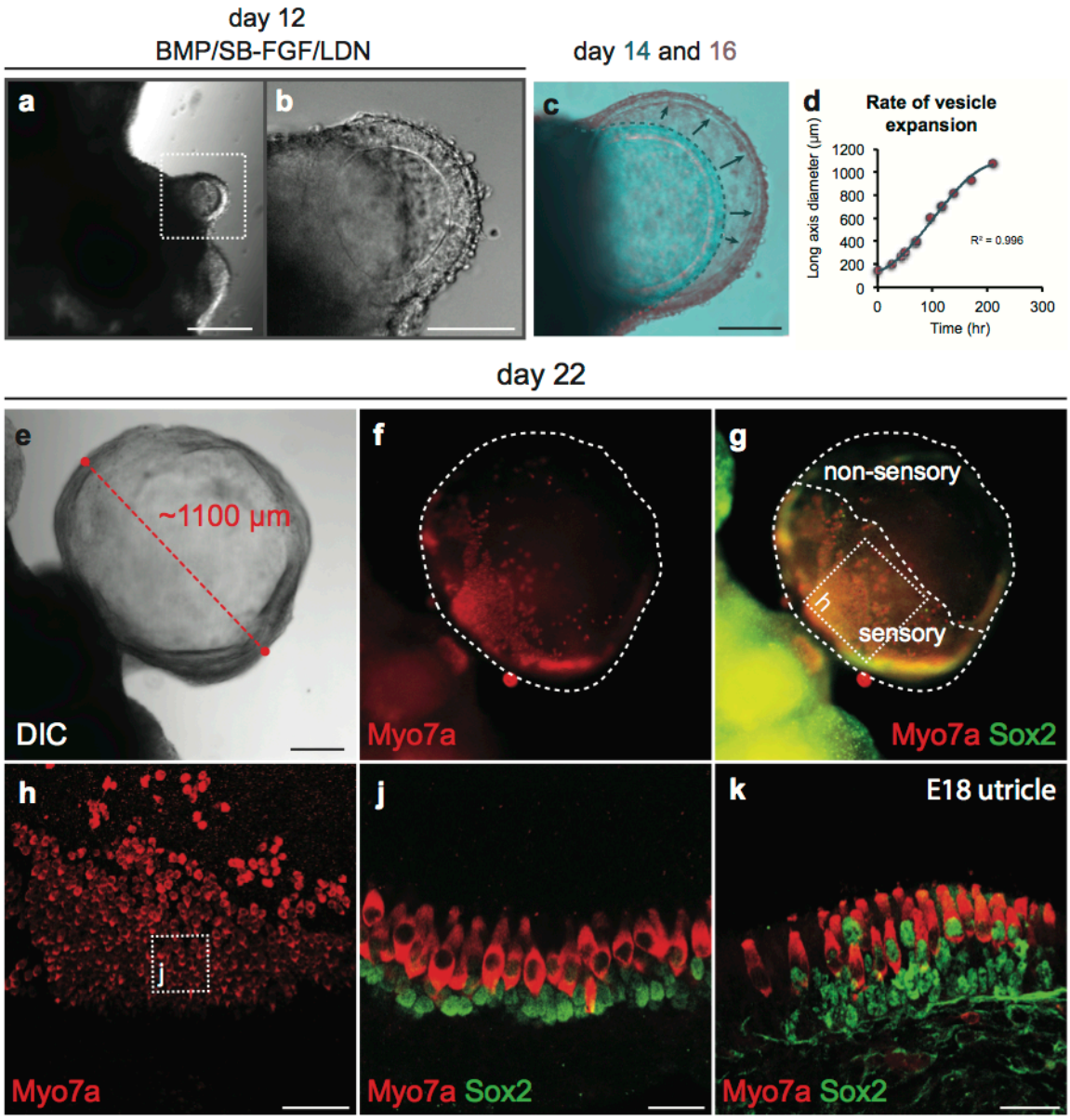

Supplementary Figure 15. Expansion of hair cell-containing vesicles (d12-22).
a, **b**, We tracked the development of a vesicle that erupted on the surface of the aggregate unusually early at day 12. **c-e**, The long-axis diameter of the aggregate grew to be ~1100 µm by day 22, which is on the scale of a typical adult mouse utricle (P30; see Li et al. 2008 for comparison)[9]. **f-i**, Whole-mount immunohistochemistry showed that a "sensory" region of the vesicle contained an epithelium with $Sox2^+$ supporting cells and a dense population of $Myo7a/Sox2^+$ hair cells, while a "non-sensory" region contained dispersed clusters of sensory epithelium. **i**, **j**, The regional organization and size of the vesicle is comparable to the E18 utricle (shown in **k**) and saccule (not shown). Scale bars, 250 µm (**a, e-g**), 100 µm (**b, c, h**), 25 µm (**i**, **j**).

Note the similarities between these stem cell-derived vesicles and cysts generated by maintaining utricular explants in 3D culture (reported in Gaboyard et al., 2005)[10].

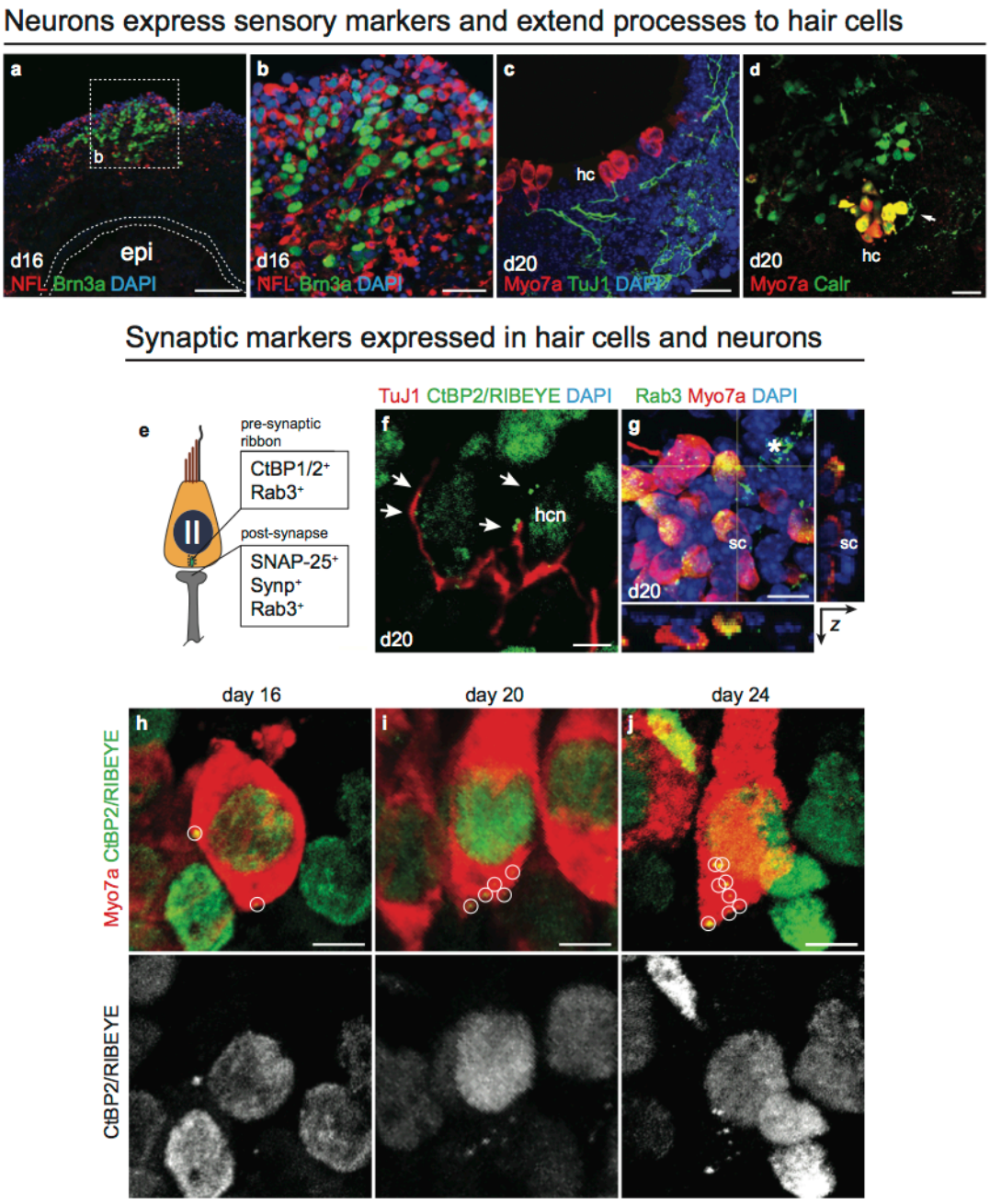

Supplementary Figure 16. Sensory neurons and synapse formation in BMP/SB-FGF/LDN aggregates (d16-20).

Clusters of neurofilament/Brn3a$^+$ (**a, b**) neurons were found in day 16 aggregates. **c**, TuJ1$^+$ neuronal processes were observed extending toward Myo7a$^+$ hair cells (hc). **d,** Calretinin$^+$ neurons extended processes toward and made contact (arrow) with hair cells. Calretinin expression is associated with sensory neurons of the inner ear vestibular and auditory ganglia. **e**, Schematic of Type II vestibular hair cells highlighting several pre- and post-synaptic markers at ribbon synapses. **f**, TuJ1$^+$ neuronal processes are associated with CtBP2/RIBEYE$^+$ puncta in stem cell-derived hair cells. Note that the CtBP2/RIBEYE antibody labels ribbon synapses and hair cell nuclei (hcn). **g**, Rab3$^+$puncta were found on the basal end of Myo7a$^+$ hair cells and

neuronal process (asterisks). Supporting cells (sc) have been labeled for orientation **h-i**, Representative images showing the increase in CtBP2/RIBEYE^{+} puncta (white circles) found on hair cells over time in culture (d16, 20 and 24). Scale bars, 50 μm (**a**), 25 μm (**b-d**), 10 μm (**g**), 5 μm (**f, h-j**).

Note that we did not detect markers of mature calyceal synapses in day 20 aggregates (i.e. Caspr1/2), which would indicate the development of Type I vestibular hair cells (data not shown). This result, however, does not preclude the later development of Type I hair cells in these cultures.

Supplementary Video Legends

Supplementary Video 1. 3D reconstruction of a vesicle lined with Myo7a/Sox2^{+} hair cells and Sox2^{+} supporting cells. (MOV; 12.7 MB)
A series of images and an animated 3D reconstruction of the vesicle seen in Fig. 3.

Supplementary Video 2. Characteristics of sensory epithelia displayed in vesicles containing hair cells. (MOV; 28.8 MB)
A series of images highlighting (1) the F-actin+ banding pattern on the luminal surface of each hair cell vesicle and (2) the F-actin/Myo7a+ stereocilia-like protrusions emanating from the apical surface of hair cells into the lumen. Additionally, a 3D reconstruction of the sensory epithelium rotates in order to provide multiple views of the protruding stereocilia at day 20. A second 3D reconstruction of an epithelium at day 24 is stained for F-actin and acetylated-a-Tubulin to visualize more mature stereocilia bundles and kinocilium, respectively.

Supplementary References

1. Suga, H. *et al.* Self-formation of functional adenohypophysis in three-dimensional culture. *Nature* **480**, 57–62 (2011).
2. Wataya, T. *et al.* Minimization of exogenous signals in ES cell culture induces rostral hypothalamic differentiation. *Proc Natl Acad Sci USA* **105**, 11796–11801 (2008).
3. Muguruma, K. *et al.* Ontogeny-recapitulating generation and tissue integration of ES cell-derived Purkinje cells. *Nat Neurosci* **13**, 1171–1180 (2010).
4. Eiraku, M. *et al.* Self-organized formation of polarized cortical tissues from ESCs and its active manipulation by extrinsic signals. *Cell Stem Cell* **3**, 519–532 (2008).
5. Eiraku, M. *et al.* Self-organizing optic-cup morphogenesis in three-dimensional culture. *Nature* **472**, 51–56 (2011).
6. Kamiya, D. *et al.* Intrinsic transition of embryonic stem-cell differentiation into neural progenitors. *Nature* **470**, 503–509 (2011).
7. Oshima, K. *et al.* Mechanosensitive Hair Cell-like Cells from Embryonic and Induced Pluripotent Stem Cells. *Cell* **141**, 704–716 (2010).
8. Meyers, J. R. *et al.* Lighting up the senses: FM1-43 loading of sensory cells through nonselective ion channels. *Journal of Neuroscience* **23**, 4054–4065 (2003).
9. Li, A., Xue, J. & Peterson, E. H. Architecture of the mouse utricle: macular organization and hair bundle heights. *J Neurophysiol* **99**, 718–733 (2008).
10. Gaboyard, S. *et al.* Three-dimensional culture of newborn rat utricle using an extracellular matrix promotes formation of a cyst. *Neuroscience* **133**, 253–265 (2005).